Electronic Structure and Bonding Situation in M_2O_2 (M = Be, Mg, Ca) Rhombic Clusters

Wan-Lu Li,[†] Jun-Bo Lu,[†] Lili Zhao,[&] Robert Ponec,[*,‡] David L. Cooper[¶], Jun Li[*,†] and Gernot Frenking[*,&,%]

[†]Department of Chemistry and Key Laboratory of Organic Optoelectronics & Molecular Engineering of Ministry of Education, Tsinghua University, Beijing 100084, China. Email: junli@tsinghua.edu.cn

[¶]Department of Chemistry, University of Liverpool, Liverpool L69 7ZD, UK

[‡]Institute of Chemical Process Fundamentals, Czech Academy of Sciences Prague 6, Suchdol 2, 165 02 Czech Republic. Email: PONEC@icpf.cas.cz

[&]Institute of Advanced Synthesis, School of Chemistry and Molecular Engineering, Jiangsu National Synergetic Innovation Center for Advanced Materials, Nanjing Tech University, Nanjing 211816, China

[%]Fachbereich Chemie, Philipps-Universität Marburg, Hans-Meerwein-Strasse 4, D-35043 Marburg, Germany. Email: frenking@chemie.uni-marburg.de

Abstract. Quantum chemical calculations using ab initio methods at the CCSD(T) level and density functional theory have been carried out for the title molecules. The electronic structures of the molecules were analyzed with a variety of charge- and energy decomposition methods. The equilibrium geometries of the M_2O_2 rhombic clusters exhibit very short distances between the transannular metal atoms M = Be, Mg, Ca. The calculated distances are close to standard values between double and triple bonds but there are no chemical M-M bonds. The metal atoms M carry large positive partial charges, which are even bigger than in diatomic MO. The valence electrons of M are essentially shifted toward oxygen in M_2O_2, which makes it possible that there is practically no electronic charge in the region between the metal atoms. The bond dissociation energies for fragmentation of M_2O_2 into two metal oxides MO are very large. The metal-oxide bonds in the rhombic clusters are shorter and stronger than in diatomic MO. A detailed analysis of the electronic structure suggests that there is no significant direct M-M interaction in the M_2O_2 rhombic clusters, albeit weak three-center M-O-M bonding.

1. Introduction

Covalent bonds are usually associated with interatomic distances that give rise to standard values for single and multiple bonds.[1-3] Very short distances are typically considered as indicator for high bond order and relatively strong bonds. A recent joint experimental and theoretical study reported an unusual situation in which a Be_2O_2 rhombus stabilized by two noble gas atoms (Ng-Be_2O_2-Ng′) features a very short metal-metal distance of ~1.75 Å that conforms to a standard value between double and triple bond and yet, no direct Be-Be bonding was found.[4] Calculations showed that the Be_2O_2 cluster changes very little when it is coordinated by the noble gas atoms, which means that the bare Be_2O_2 species features a short distance/no bond scenario. A similar situation was reported for other Be-Be molecules[5-6] and also for compounds with short Si-Si distances.[7-11]

The cited examples suggest unusual electronic structures in the molecules, which deserve to be analyzed in more detail with modern quantum chemical methods. We were curious to see how the peculiar (no)bonding situation shows up in a variety of methods for bonding analysis and whether it is also found in the heavier homologues of beryllium. To this end we calculated the rhombic clusters M_2O_2 of the earth alkaline elements M = Be, Mg, Ca using the previous[4] study of Be_2O_2 as reference. We have employed for this purpose a range of widely used theoretical tools, including quantum theory of atoms in molecules (QTAIM),[12] natural bond order (NBO) analysis,[13] domain-averaged Fermi hole (DAFH) analysis,[14-20] energy decomposition analysis in conjunction with natural orbitals for chemical valence (EDA-NOCV),[21-24] and adaptive natural density partitioning (AdNDP),[25] that have proved useful in revealing the nature of the bonding in various molecules with non-trivial bonding patterns.

2. Theoretical methods

Full geometry optimizations of the M_2O_2 molecules in D_{2h} symmetry were performed using coupled-cluster theory[26-33] with single and double excitation (CCSD) in conjunction with all-electron triple-zeta cc-pVTZ basis set[34-35] as implemented in the MOLPRO 2012 software package[36] and available at the EMSL basis set exchange.[37] Vibrational frequency calculations were carried out, which show that the optimized

species are minima on the potential energy surface. The reaction energies for the dimerization reaction 2 MO → M_2O_2 were calculated at the CCSD(T)/cc-pVTZ level using the CCSD/cc-pVTZ optimized geometries. The partial charges and Wiberg bond indices were calculated with the NBO program 6.1 using the program package Gaussian 16.[38] The QTAIM analysis was performed using AIMAll.[39] The EDA-NOCV calculations were performed with density functional theory (DFT) at the BP86[40-41]/TZ2P[42] level using the Amsterdam Density Functional (ADF 2016.101) program.[43]

Further visual insights into the nature of the bonding were obtained by performing isopycnic localization[44] of the CCSD/cc-pVTZ natural orbitals, by calculating three-center bonding indices, and by carrying out domain-averaged Fermi hole (DAFH) analysis[14-20] for the M and O QTAIM domains, using our own codes. Such DAFH analysis formally requires use of the pair density but, when that is not available, we may use instead an approximation[45] that requires only the natural orbital occupation numbers.[18] Additionally, AdNDP analysis[25] was performed at the B3LYP/cc-pVTZ level using the Multiwfn 3.4.0 program[46].

3. Results and Discussion

Figure 1 shows the optimized geometries of the diatomic molecules MO and the rhombic structures M_2O_2. The calculated bond lengths of the monomers are in good agreement with the experimental values.[47] The dimers M_2O_2 possess rather acute angles at oxygen M-O-M, which are well below 90º for Be_2O_2 and Mg_2O_2 while Ca_2O_2 is a near square with a Ca-O-Ca angle of 91.4º. The M-O distances in M_2O_2 are stretched by ~0.1 - 0.2 Å with regard to the monomers. The M-M distances in all M_2O_2 species are quite short. The Be-Be distance of 1.717 Å is close to a standard value for a triple bond (1.70 Å), the Mg-Mg distance of 2.367 Å is even shorter than the reference value for a triple bond (2.54 Å) while the Ca-Ca distance (2.954 Å) is close to a double bond length (2.94 Å).[1-3] The standard values for single, double and triple bonds M-M are shown in Table 1.

Figure 1, Table 1

The dimerization energies of the process 2 MO → M_2O_2 are very large. Table 2

shows that the bond dissociation energy (BDE) of Be_2O_2 is D_e = 162.7 kcal/mol. Somewhat smaller but still very large BDEs are calculated for Mg_2O_2 (D_e = 130.2 kcal/mol) and Ca_2O_2 (D_e = 121.5 kcal/mol). The positive values for the atomic partial charges at the metal atoms in MO increase even further in M_2O_2 (Table 2), which indicates a higher ionic character in the dimers. This is corroborated by the Wiberg bond indices of the M-O bonds P(M-O), which become much smaller in the dimers (0.32 - 0.56) than in the monomers (0.89 - 1.16). The calculated bond orders P(M-M) are very small in spite of the very short M-M distances. The theoretical values of P(M-M) are between 0.03 and 0.06, which indicates that there is hardly any covalent M-M interaction.

Table 2, Figure 2

The absence of M-M bonding interactions in the rhombic dimers M_2O_2 is further supported by QTAIM analysis of the electronic structures. Figure 2 shows the Laplacian distributions $\nabla^2\rho(r)$ along with the bond paths and the critical points of the molecules. There are areas of charge concentration at the valence space around the oxygen atoms ($\nabla^2\rho(r) > 0$, red dashed lines) while the metal atoms exhibit charge depletion in the valence space ($\nabla^2\rho(r) < 0$, blue solid lines). The red dashed lines around the nuclei of Mg and Ca indicate the outermost core electrons. The 1s core electrons are omitted. The Laplacian distributions of M_2O_2 are in agreement with the calculated partial charges. There are four bond critical points (bcp) and four bond paths for the M-O bonds in M_2O_2 but there is no bcp nor a bond path along the M-M axis. There is a bcp and a bond path along the O-O axis in Be_2O_2 and Mg_2O_2, although the oxygen-oxygen distances are very long. This does not indicate a genuine chemical bond[48] but it rather comes from the gradient of the electronic charge in the plane of the dimers. There is no O-O bcp in Ca_2O_2. There are two ring critical points close to the O-O bcp in Be_2O_2 and Mg_2O_2, because the topology of the charge distributions exhibits a bicyclic structure. The topology of the Laplacian distribution of Ca_2O_2 suggests a rectangular cyclic structure. The most important result of the QTAIM calculations is the support of the absence of M-M bonding in the rhombic dimers M_2O_2.

Table 3

We analyzed the electronic structure with the combined charge- and energy decomposition analysis EDA-NOCV. Table 3 shows the numerical results of the

calculation where two MO monomers are taken as interacting fragments. The calculated BDEs at the BP86(D3)/TZ2P+ level have very similar values as the CCSD(T)/cc-pVQZ results. The intrinsic interaction energies ΔE_{int} at BP86(D3)/TZ2P+ are only slightly smaller larger than the BDEs, because the preparation energies ΔE_{prep}, which are due to the bond lengthening of the MO monomers in M_2O_2, are rather small. Thus, the ΔE_{int} values may be taken for analyzing the nature of the dimerization process. The calculations suggest that they have a higher electrostatic (ionic) than covalent character. The orbital interactions ΔE_{orb} provide 35% - 43% of the total attraction. The most interesting information comes from the pairwise interactions of ΔE_{orb}. Table 3 gives the list of the six strongest pairs $\Delta E_{orb(1)}$ - $\Delta E_{orb(6)}$, which comprise 97% - 96% of ΔE_{orb}. The connected deformation densities $\Delta\rho$ and the associated most important interacting orbitals of Be_2O_2 are shown in Figure 3. The deformation densities $\Delta\rho$ and the interacting orbitals of the heavier homologues Mg_2O_2 and Ca_2O_2 are very similar. They are given in Figures S1 and S2 of Supporting Information.

Figure 3

The strongest pair interaction $\Delta E_{orb(1)}$ comes from HOMO→LUMO donation that involves the in-plane π component of the HOMO (Figure 3). The second strongest donation $\Delta E_{orb(1)}$ arises from HOMO-1→LUMO donation. The associated deformation densities illustrate the formation of the new Be-O bonds. Note that there is in both cases also a blue area of charge accumulation at the centre of ring. This might be the reason that the QTAIM analysis identifies an O-O bcp (Fig. 2a). The pair contributions $\Delta E_{orb(3)}$ and $\Delta E_{orb(5)}$ indicate out-of-plane π interactions from the π' component of the HOMO into the π'-antibonding LUMO+1 ($\Delta E_{orb(3)}$) and the energetically high-lying LUMO-10, which comes from the polarization functions. The latter contribution signals a comparatively weak π' delocalization. The pair contribution $\Delta E_{orb(4)}$ comes from the in-plane π component of the HOMO of the fragments, which interact with the LUMO+1 and LUMO+3. The weakest pair contribution $\Delta E_{orb(6)}$ is due to the charge donation from the HOMO-1 into a mixing of the LUMO+4 and HOMO, which is partly depleted in the pair interactions $\Delta E_{orb(1)}$ and $\Delta E_{orb(4)}$.

In order to reveal further visual insights into the nature of the bonding interactions, we carried out isopycnic localization of the CCSD/cc-pVTZ natural orbitals. We note that the resulting localized natural orbitals (LNOs) are necessarily the same as the

functions obtained when applying DAFH analysis for the hole averaged over the union of all the QTAIM domains in the molecule. It proved straightforward by visual inspection to identify the eight valence LNOs for each cluster. As can be seen from Figure 4, four of the valence LNOs correspond to fairly localized M-O σ bonds that form the main skeleton of the cluster and two σ valence LNOs correspond to distorted $2s^2$ quasi-lone pairs on O atoms. The two remaining valence LNOs take the form of distorted O($2p_\pi$) functions that are sufficiently deformed towards neighboring M atoms so as to suggest the existence of some degree of delocalized three-center two-electron (3c-2e) π bonding within the M-O-M moieties. As such, it proves informative to examine the values of appropriate 3c M-O-M bonding indices.

Figure 4

From the plethora of definitions of correlated 3c indices,[49-54] we chose the QTAIM-generalized one reported by Cooper et al.[54] that has the advantage of maintaining exact normalization. Although relatively small, the resulting M-O-M 3c bond indices (0.013, 0.017 and 0.041 for M=Be, Mg, Ca) are not negligible. Further analysis shows that the main contributions do in fact arise from the two adjacent M-O σ bonds, with smaller contributions from the deformed O($2p_\pi$) functions and practically none from the distorted O($2s^2$) quasi-lone pairs. The observation here of an in-phase combination of positive contributions to 3c indices from 3c-4e σ and 3c-2e π interactions (see Table S1 in the Supporting Information), even though 3c-4e situations more usually correspond to negative values, can easily be rationalized using simple Hückel-like models.[20]

For a hole averaged over a single QTAIM domain, DAFH analysis provides information about the core and lone pairs retained in that fragment as well as about the broken or dangling valences that are created by the formal splitting of bonds so as to isolate this particular fragment from the rest of the molecule. The broken valences arising from DAFH analysis at the CCSD/cc-pVTZ level for the M and O QTAIM domains are shown in Figure 5, together with their associated populations, n_M and n_O. For all three clusters, the close visual resemblance of the complementary functions associated with the M and O fragments of the formally broken M-O bond indicates a character of more-or less ordinary shared electron pair bonds, with $n_M + n_O \approx 2$. On the other hand, the considerable differences between n_M and n_O for a given cluster indicate

that the bonding electron pairs of the M-O bonds are shared extremely unevenly, consistent with the high polarity of the bonding in these systems.

Figures 5, 6

The corresponding pictures for LNOs and DAFH functions at the B3LYP and full-valence CASSCF levels (in the latter case explicitly using the pair density) turn out to be little changed from those shown in Figures 4 and 5 (see Figures S3-S4 in the Supporting Information). Independent corroboration for the distribution of electrons revealed by the various sets of valence LNOs is provided by the results of AdNDP analysis, shown in Figure 6, which also detects the M-O σ bonds, the quasi-$2s^2$ lone pairs on O atoms and the distorted π functions in the M-O-M moieties.

4. Summary

The results of this work may be summarized as follows. The equilibrium geometries of the M_2O_2 rhombic clusters exhibit very short distances between the transannular metal atoms M = Be, Mg, Ca. The calculated distances are close to standard values between double and triple bonds but there are no chemical M-M bonds. The metal atoms M carry large positive partial charges, which are even bigger than in diatomic MO. The valence electrons of M are essentially shifted toward oxygen in M_2O_2, which makes it possible that there is practically no electronic charge in the region between the metal atoms. The bond dissociation energies for fragmentation of M_2O_2 into two metal oxides MO are very large. The metal-oxide bonds in the rhombic clusters are shorter and stronger than in diatomic MO. A detailed analysis of the electronic structure suggests that there is no significant direct M-M interaction in the M_2O_2 rhombic clusters, but there is evidence for a small degree of three-center bonding character in the M-O-M moieties.

Supporting Information. Two figures S1 and S2 showing the deformation densities Δρ and the interacting orbitals of the dimers Mg_2O_2 and Ca_2O_2. Figures S3 and S4 showing the valence LNOs at the B3LYP/cc-pVTZ and CASSCF/cc-pVTZ levels of theory. Table S1 giving the contributions by symmetry to the total QTAIM-generalized M-O-M 3c bond indices.

Acknowledgements

We thank Prof. W. H. Eugen Schwarz and Mingfei Zhou for invaluable discussions. This work was supported by National Natural Science Foundation of China (grant nos. 21590792 and 21433005). Various calculations were performed using supercomputers at the Computer Network Information Center, Chinese Academy of Sciences, Tsinghua National Laboratory for Information Science and Technology, and Lüliang Tianhe-2 Supercomputing Center. Further calculations were carried out using resources at the Institute of Chemical Process Fundamentals and at the University of Liverpool.

References

1. Pyykkö, P.; Riedel, S.; Patzschke, M. Triple-Bond Covalent Radii. *Chem. Eur. J.* **2005**, *11*, 3511-3520.
2. Pyykkö, P.; Atsumi, M. Molecular Single-Bond Covalent Radii for Elements 1–118. *Chem. Eur. J.* **2009**, *15*, 186-197.
3. Pyykkö, P.; Atsumi, M. Molecular Double-Bond Covalent Radii for Elements Li–E112. *Chem. Eur. J.* **2009**, *15*, 12770-12779.
4. Zhang, Q.; Li, W.-L.; Zhao, L.; Chen, M.; Zhou, M.; Li, J.; Frenking, G., A Very Short Be–Be Distance but No Bond: Synthesis and Bonding Analysis of Ng–Be_2O_2–Ng′ (Ng, Ng′=Ne, Ar, Kr, Xe). *Chem-Eur. J.* **2017,** *23*, 2035-2039.
5. Cui, Z.-H.; Yang, W.-S.; Zhao, L.; Ding, Y.-H.; Frenking, G. Unusually Short Be−Be Distances with and without a Bond in Be_2F_2 and in the Molecular Discuses Be_2B_8 and $Be_2B_7^-$. *Angew. Chem., Int. Ed.* **2016**, *55*, 7841-7846.
6. Yuan, C.; Zhao, X.-F.; Wu, Y.-B.; Wang, X. Ultrashort Beryllium−Beryllium Distances Rivalling Those of Metal−Metal Quintuple Bonds Between Transition Metals. *Angew. Chem. Int. Ed.* **2016**, *55*, 15651-15655.
7. Gau, D.; Nougué, R.; Saffon-Merceron, N.; Baceiredo, A.; De Cózar, A.; Cossío, F. P.; Hashizume, D.; Kato, T. Donor-Stabilized 1,3-Disila-2,4-diazacyclobutadiene with a Nonbonded Si···Si Distance Compressed to a Si=Si Double Bond Length. Angew. Chem., Int. Ed. 2016, 55, 14673-14677.
8. Fink, M. J.; Haller, K. J.; West, R.; Michl, J. Tetramesitylcyclodisiloxane: a cyclic siloxane with an unusual structure. *J. Am. Chem. Soc.* **1984**, *106*, 822-823.
9. Michalczyk, M. J.; Fink, M. J.; Haller, K. J.; West, R.; Michl, J. Structural and chemical properties of 1,3-cyclodisiloxanes. *Organomet.* **1986**, *5*, 531-538.
10. Yokelson, H. B.; Millevolte, A. J.; Adams, B. R.; West, R. Bonding in 1,3-cyclodisiloxanes: silicon-29 NMR coupling constants in disilenes and 1,3-cyclodisiloxanes. *J. Am. Chem. Soc.* **1987**, *109*, 4116-4118.
11. Jemmis, E. D.; Kumar, P. N. V. P.; Kumar, N. R. S. Structure and bonding in $(R_2SiX)_2$ molecules (X = O, NH, CH_2, or S; R = H). *J Chem Soc, Dalton Trans.* **1987**, 271-273.
12. Bader, R. F. W. Atoms in Molecules, A Quantum Theory; Oxford University Press,

Oxford (1990).

13. Weinhold, F.; Landis, C. R., *Valency and Bonding. A Natural Bond Orbital Donor-Acceptor Perspective*. Cambridge University Press: Cambridge, U. K., 2005.
14. Ponec, R. Electron pairing and chemical bonds. Chemical structure, valences and structural similarities from the analysis of the Fermi holes. *J. Math. Chem.* **1997**, *21*, 323-333.
15. Ponec, R.; Duben, A. J. Electron pairing and chemical bonds: Bonding in hypervalent molecules from analysis of Fermi holes. *J. Comput. Chem.* **1999**, *20*, 760-771.
16. Ponec, R.; Cooper, D. L. Anatomy of bond formation. Bond length dependence of the extent of electron sharing in chemical bonds from the analysis of domain-averaged Fermi holes. *Faraday Discuss.* **2007**, *135*, 31-42.
17. Ponec, R. Structure and bonding in binuclear metal carbonyls. Classical paradigms vs. insights from modern theoretical calculations. *Comp. Theor. Chem.* **2015**, *1053*, 195-213.
18. Cooper, D. L.; Ponec, R. A one-electron approximation to domain-averaged Fermi hole analysis. *Phys. Chem. Chem. Phys.* **2008,** *10*, 1319-1329.
19. Ponec, R.; Cooper, D. L.; Savin, A. Analytic models of domain-averaged Fermi holes: A new tool for the study of the nature of chemical bonds. *Chem. Eur. J.* **2008**, *14*, 3338-3345.
20. Ponec, R.; Cooper, D. L. Insights from domain-averaged Fermi hole (DAFH) analysis and multicenter bond indices into the nature of Be(0) bonding. *Struct. Chem.* **2017**, *28*, 1033-1043.
21. Ziegler, T.; Rauk, A. A theoretical study of the ethylene-metal bond in complexes between copper(1+), silver(1+), gold(1+), platinum(0) or platinum(2+) and ethylene, based on the Hartree-Fock-Slater transition-state method. *Inorg. Chem.* **1979**, *18*, 1558-1565.
22. Michalak, A.; Mitoraj, M.; Ziegler, T. Bond Orbitals from Chemical Valence Theory. *J. Phys. Chem. A* **2008**, *112*, 1933-1939.
23. Mitoraj, M. P.; Michalak, A.; Ziegler, T. A Combined Charge and Energy Decomposition Scheme for Bond Analysis. *J. Chem. Theory Comput.* **2009**, *5*, 962-975.

24. von Hopffgarten, M.; Frenking, G., Energy decomposition analysis. *WIREs Comput. Mol. Sci.* **2017,** DOI: 10.1002/wcms.1345.
25. Zubarev, D. Y.; Boldyrev, A. I., Developing paradigms of chemical bonding: adaptive natural density partitioning. *Phys. Chem. Chem. Phys.* **2008,** *10*, 5207-5217.
26. Cizek, J. On the Correlation Problem in Atomic and Molecular Systems. Calculation of Wavefunction Components in Ursell‐Type Expansion Using Quantum‐Field Theoretical Methods. *J. Chem. Phys.* **1966**, *45*, 4256-4266.
27. Pople, J. A.; Krishnan, R.; Schlegel, H. B.; Binkley, J. S. Electron correlation theories and their application to the study of simple reaction potential surfaces. *Int. J. Quantum Chem.* **1978**, *14*, 545-560.
28. Bartlett, R. J.; Purvis, G. D. Many-body perturbation theory, coupled-pair many-electron theory, and the importance of quadruple excitations for the correlation problem. *Int. J. Quantum Chem.* **1978**, *14*, 561-581.
29. Purvis, G. D.; Bartlett, R. J. A full coupled‐cluster singles and doubles model: The inclusion of disconnected triples. *J. Chem. Phys.* **1982**, *76*, 1910-1918.
30. Raghavachari, K.; Trucks, G. W.; Pople, J. A.; Head-Gordon, M. A fifth-order perturbation comparison of electron correlation theories. *Chem. Phys. Lett.* **1989**, *157*, 479-483.
31. Bartlett, R. J.; Watts, J. D.; Kucharski, S. A.; Noga, J. Non-iterative fifth-order triple and quadruple excitation energy corrections in correlated methods. *Chem. Phys. Lett.* **1990**, *165*, 513-522.
32. Hampel, C.; Peterson, K. A.; Werner, H.-J. A comparison of the efficiency and accuracy of the quadratic configuration interaction (QCISD), coupled cluster (CCSD), and Brueckner coupled cluster (BCCD) methods. *Chem. Phys. Lett.* **1992**, *190*, 1-12.
33. Watts, J. D.; Gauss, J.; Bartlett, R. J. Coupled‐cluster methods with noniterative triple excitations for restricted open‐shell Hartree–Fock and other general single determinant reference functions. Energies and analytical gradients. *J. Chem. Phys.* **1993**, *98*, 8718-8733.
34. Dunning Jr., T. H., Gaussian basis sets for use in correlated molecular calculations. I. The atoms boron through neon and hydrogen. *J. Chem. Phys.* **1989,** *90*, 1007-1023.

35. Feller, D. The role of databases in support of computational chemistry calculations. *J. Comp. Chem.* **1996,** *17*, 1571-1586.
36. Werner, H.-J.; Knowles, P. J.; Knizia, G.; Manby, F. R.; Schütz, M.; and others, http://www.molpro.net, 2012.
37. K. Schuchardt, B. Didier, T. Elsethagen, L.-S. Sun, V. Gurumoorthi, J. Chase, J. Li, T. L. Windus, "Basis Set Exchange: A Community Database for Computational Sciences", *J. Chem. Inf. Model.* **2007**, *47*, 1045-1052. https://bse.pnl.gov/bse/portal.
38. Gaussian 16, Revision C.01, Frisch, M. J.; Trucks, G. W.; Schlegel, H. B.; Scuseria, G. E.; Robb, M. A.; Cheeseman, J. R.; Scalmani, G.; Barone, V.; Mennucci, B.; Petersson, G. A.; et al. Gaussian, Inc.: Wallingford, CT, 2017.
39. AIMAll (Version 17.01.25), Keith, T. A., TK Gristmill Software, Overland Park KS, USA, 2017 (aim.tkgristmill.com)
40. Becke, A. D. Density-functional exchange-energy approximation with correct asymptotic behavior. *Phys. Rev. A* **1988**, *38*, 3098-3100.
41. Perdew, J. P. Density-functional approximation for the correlation energy of the inhomogeneous electron gas. *Phys. Rev. B* **1986**, *33*, 8822-8824.
42. van Lenthe, J. H.; Baerends, E. J. Optimized Slater-type basis sets for the elements 1–118. *J. Comput. Chem*. **2003**, *24*, 1142-1156.
43. ADF, 2016.101, SCM, Theoretical Chemistry, Vrijie Universiteit, Amsterdam, The Netherlands, (http://www.scm.com).
44. Cioslowski, J. Isopycnic orbital transformations and localization of natural orbitals. *Int. J. Quantum Chem.* **1990,** *38(S24)*, 15-28.
45. Müller, A. M. K. Explicit approximate relation between reduced two- and one-particle density matrices, *Phys. Lett. A*, **1984**, *105*, 446-452.
46. Lu, T.; Chen, F. Multiwfn: A multifunctional wavefunction analyzer. *J. Comput. Chem.* **2012,** *33*, 580-592.
47. Huber, K.P., Herzberg, G. *Molecular Spectra and Molecular Structure IV. Constants of Diatomic Molecules;* Van Nostrand-Reinhold, New York, 1979.
48. R. F. W. Bader, Bond Paths Are Not Chemical Bonds, *J. Phys. Chem. A*, **2009**, *113*, 10391-10396.
49. Feixas, F.; Rodríguez-Mayorga, M.; Matito, E.; Solà, M. Three-center bonding analyzed from correlated and uncorrelated third-order reduced density matrices.

Comput. Theor. Chem. **2015,** *1053*, 173-179.

50. Feixas, F.; Solà, M.; Barroso, J. M.; Ugalde, J. M.; Matito, E. New approximation to the third-order density. Application to the calculation of correlated multicenter indices. *J. Chem. Theory Comput.* **2014,** *10*, 3055-3065.
51. Francisco, E.; Martín Pendás, A.; García-Revilla, M.; Álvarez Boto, R. A hierarchy of chemical bonding indices in real space from reduced density matrices and cumulants. *Comput. Theor. Chem.* **2013,** *1003*, 71-78.
52. Lain, L.; Torre, A.; Bochicchio, R. Studies of population analysis at the correlated level: Determination of three-center bond indices. *J. Phys. Chem. A* **2004,** *108*, 4132-4137.
53. Ponec, R.; Cooper, D. L. Generalized population analysis of three-center two-electron bonding. *Int. J. Quant. Chem.* **2004,** *97*, 1002–1011.
54. Cooper, D. L.; Penotti, F. E.; Ponec, R. Reassessing spin-coupled full generalized valence bond) descriptions of ozone using three-center bond indices. *Comput. Theor. Chem.* **2017**, *1116*, 40-49.

Captions and legends

Figure 1. Calculated geometries of monomers MO and dimers M_2O_2 (M = Be, Mg, Ca) at CCSD(T)/cc-pVTZ. Bond lengths in Å, angles in degree. Experimental values[47] are given in parentheses.

Figure 2. Plot of the Laplacian distribution $\nabla^2\rho(r)$ of Be_2O_2, Mg_2O_2 and Ca_2O_2 at the CCSD/CC-PVTZ level. Red dashed lines indicate areas of charge concentration ($\nabla^2\rho(r) < 0$) while solid blue lines show areas of charge depletion ($\nabla^2\rho(r) > 0$). The solid lines connecting the atomic nuclei are the bond paths. Green dots are bond critical points, red dots are ring critical points.

Figure 3. Plot of the deformation densities $\Delta\rho_{1\text{-}6}$ of the pairwise orbital interactions between the two BeO fragments in their singlet (S) states in Be_2O_2 and shape of the associated most important MOs of the fragments. The eigenvalues ν indicate the size of the charge flow. The direction of charge flow in the deformation densities is red→blue.

Figure 4. Valence LNOs and the corresponding occupation numbers (shown below the qualitative descriptions) at the CCSD/cc-pVTZ level of theory. Isosurface values are 0.05 (left) and 0.02 (right), as indicated.

Figure 5. Localized DAFH functions and their populations (shown below the contours) corresponding to the broken valences of M-O bonds resulting from the analysis of complementary holes averaged over M and O QTAIM domains at the CCSD/cc-pVTZ level of theory. The isosurface value is 0.05.

Figure 6. AdNDP chemical bonding analyses at the B3LYP/cc-pVTZ level of theory, with the occupation numbers shown below the qualitative descriptions. Isosurface values are 0.05 (left) and 0.02 (right), as indicated.

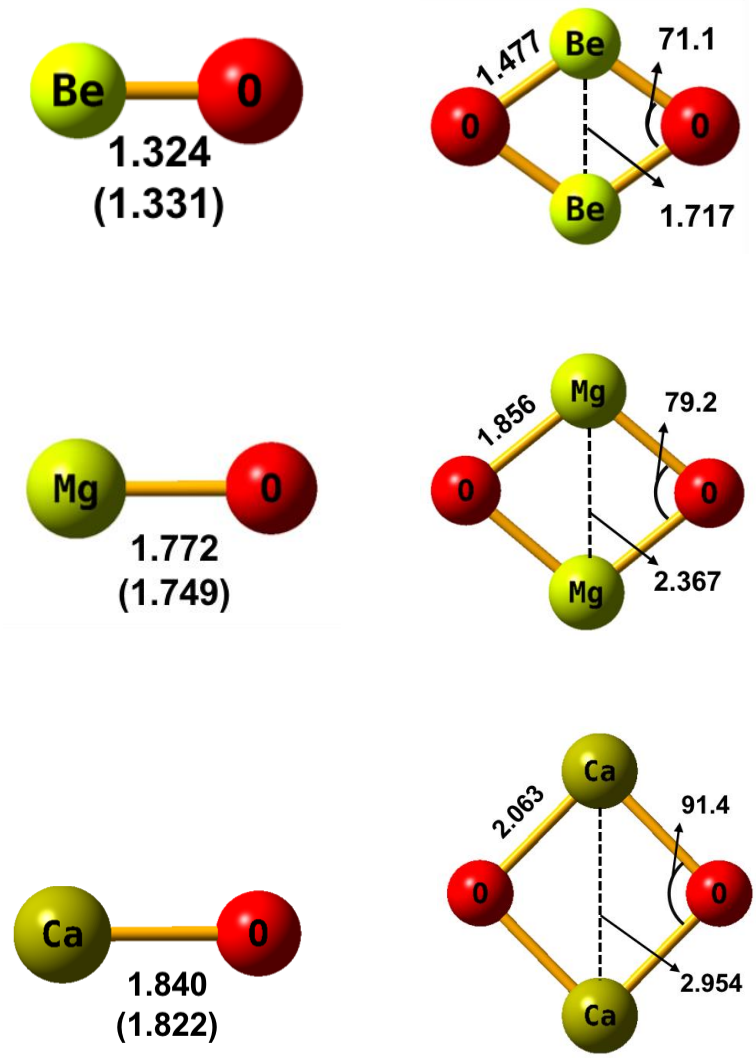
Be
O
1.324
(1.331)
1.477
Be
71.1
O
O
Be
1.717
Mg
O
1.772
(1.749)
1.856
Mg
79.2
O
O
Mg
2.367
Ca
O
1.840
(1.822)
2.063
Ca
91.4
O
O
Ca
2.954

Figure 1

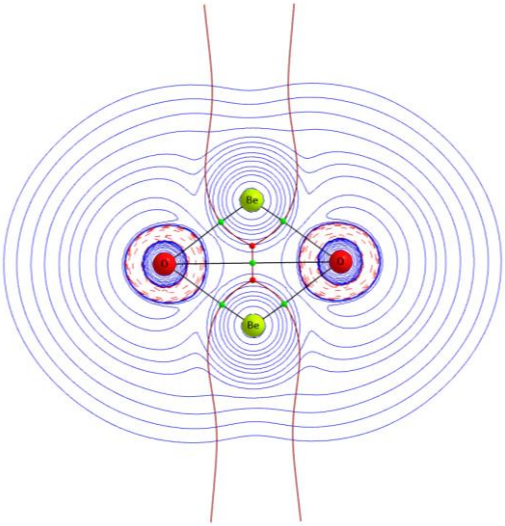

(a) Be_2O_2

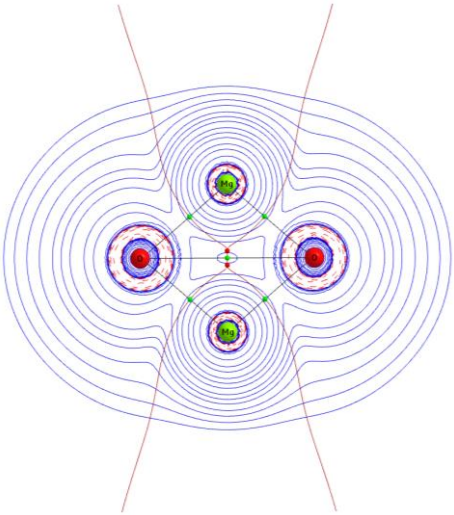

(b) Mg_2O_2

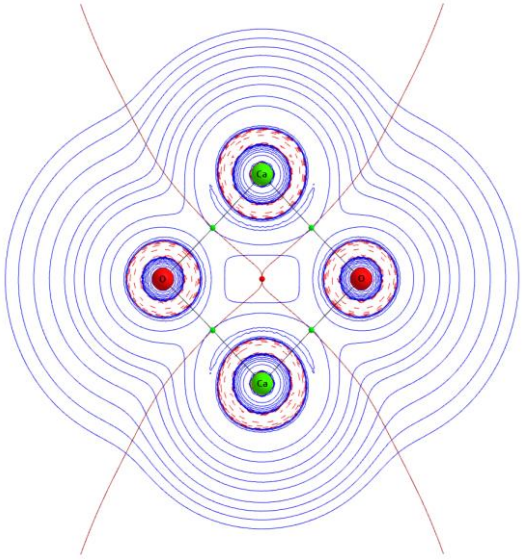

(c) Ca_2O_2

Figure 2

deformation densities Δρ	interacting MOs
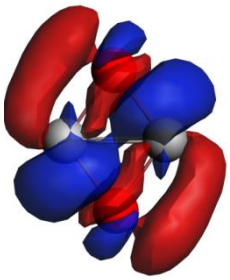 $\nu_1 = \pm 0.605$ $\Delta E_{orb(1)} = -93.4$ kcal/mol	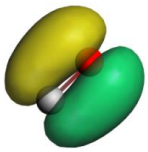 + 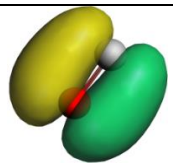 frag1-1π(HOMO) frag2-1π(HOMO) ↓ 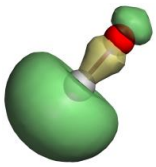 + 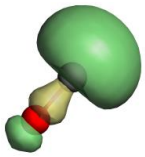 frag1-3σ(LUMO) frag2-3σ(LUMO)
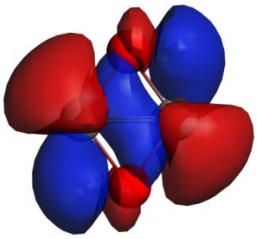 $\nu_2 = \pm 0.717$ $\Delta E_{orb(2)} = -45.6$ kcal/mol	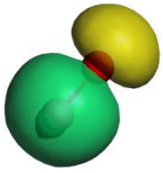 + 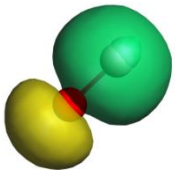 frag1-2σ(HOMO-1) frag2-2σ(HOMO-1) ↓ 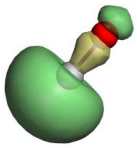 + 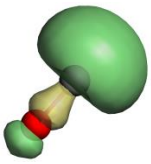 frag1-3σ(LUMO) frag2-3σ(LUMO)
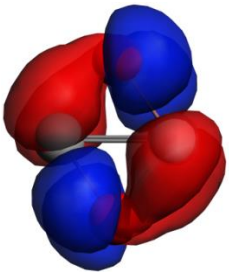 $\nu_3 = \pm 0.570$ $\Delta E_{orb(3)} = -35.8$ kcal/mol	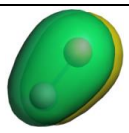 +  frag1-1π'(HOMO) frag2-1π'(HOMO) ↓ 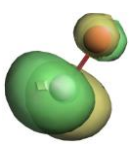 + 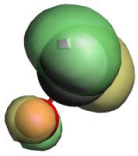 frag1-2π'(LUMO+1) frag2-2π'(LUMO+1)

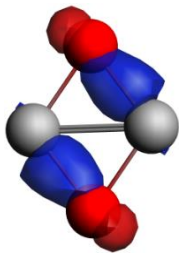

$\nu_4 = \pm 0.233$

$\Delta E_{orb(4)}$ = -15.8 kcal/mol

frag1-1π (HOMO) frag2-1π (HOMO)

↓

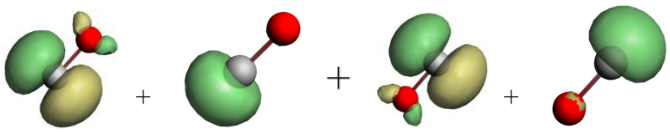

frag1-2π LUMO+1 frag1-5σ LUMO+3 frag1-2π LUMO+1 frag1-5σ LUMO+3

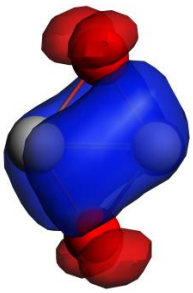

$\nu_5 = \pm 0.158$

$\Delta E_{orb(5)}$ = -7.9 kcal/mol

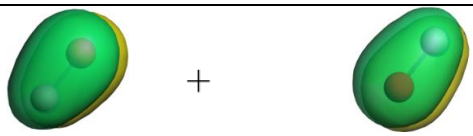

frag1-1π'(HOMO) frag2-1π'(HOMO)

↓

frag1-1δ (LUMO+10) frag2-1δ(LUMO+10)

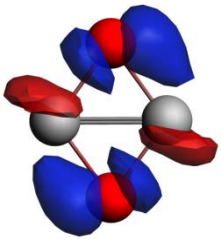

$\nu_6 = \pm 0.152$

$\Delta E_{orb(6)}$ = -5.4 kcal/mol

frag1-2σ(HOMO-1) frag2-2σ(HOMO-1)

↓

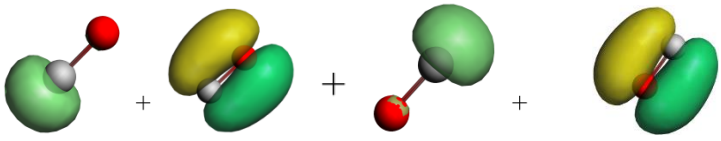

frag1-5σ (LUMO+4) frag1-1π (HOMO) frag2-5σ (LUMO+4) frag2-1π (HOMO)

Figure 3

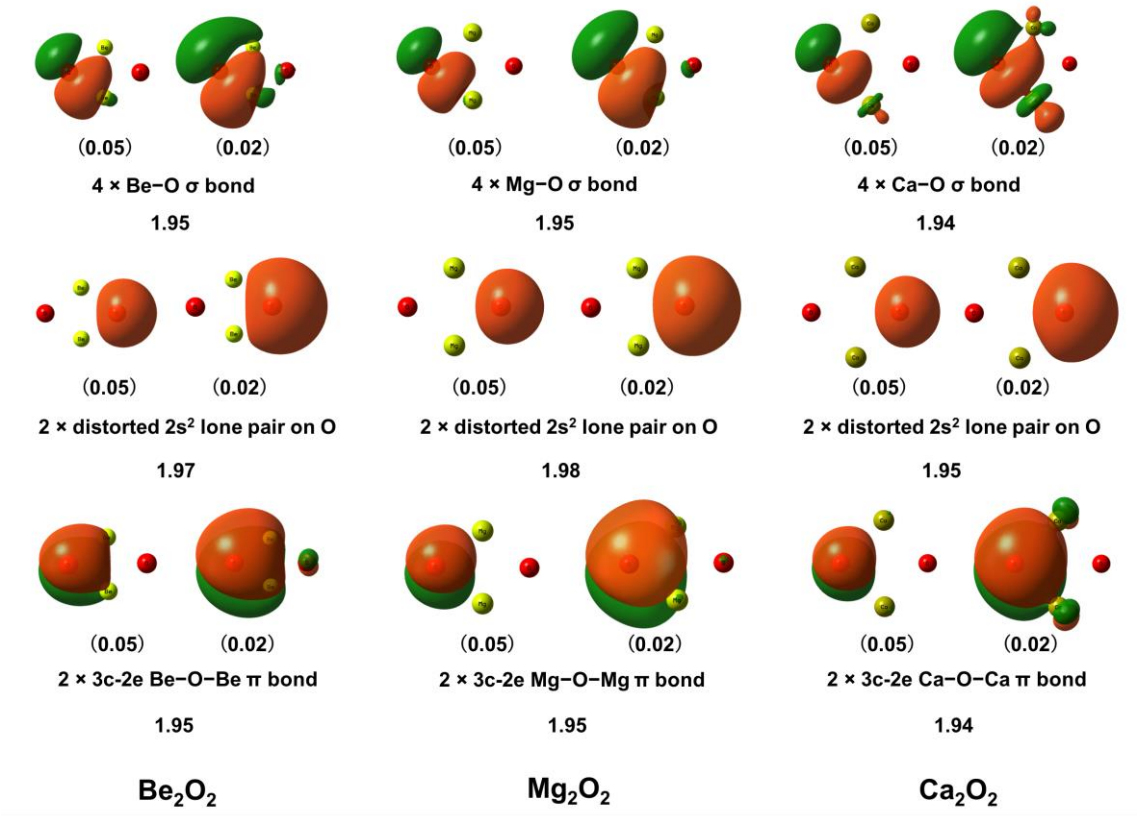
(0.05) (0.02)
4 × Be−O σ bond
1.95
(0.05) (0.02)
4 × Mg−O σ bond
1.95
(0.05) (0.02)
4 × Ca−O σ bond
1.94
(0.05) (0.02)
2 × distorted 2s² lone pair on O
1.97
(0.05) (0.02)
2 × distorted 2s² lone pair on O
1.98
(0.05) (0.02)
2 × distorted 2s² lone pair on O
1.95
(0.05) (0.02)
2 × 3c-2e Be−O−Be π bond
1.95
(0.05) (0.02)
2 × 3c-2e Mg−O−Mg π bond
1.95
(0.05) (0.02)
2 × 3c-2e Ca−O−Ca π bond
1.94
Be2O2
Mg2O2
Ca2O2

Figure 4

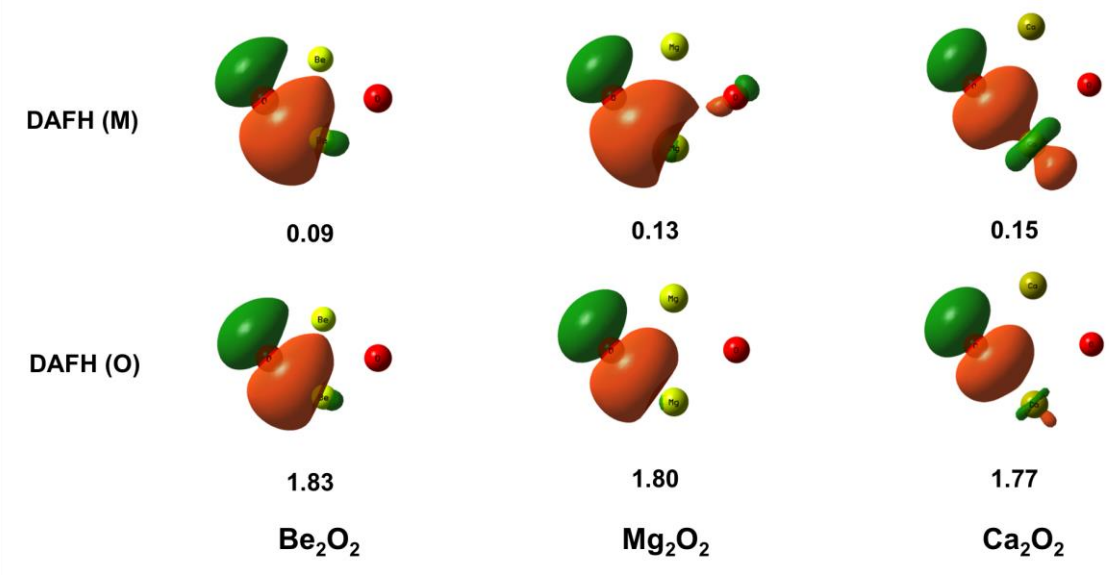

Figure 5

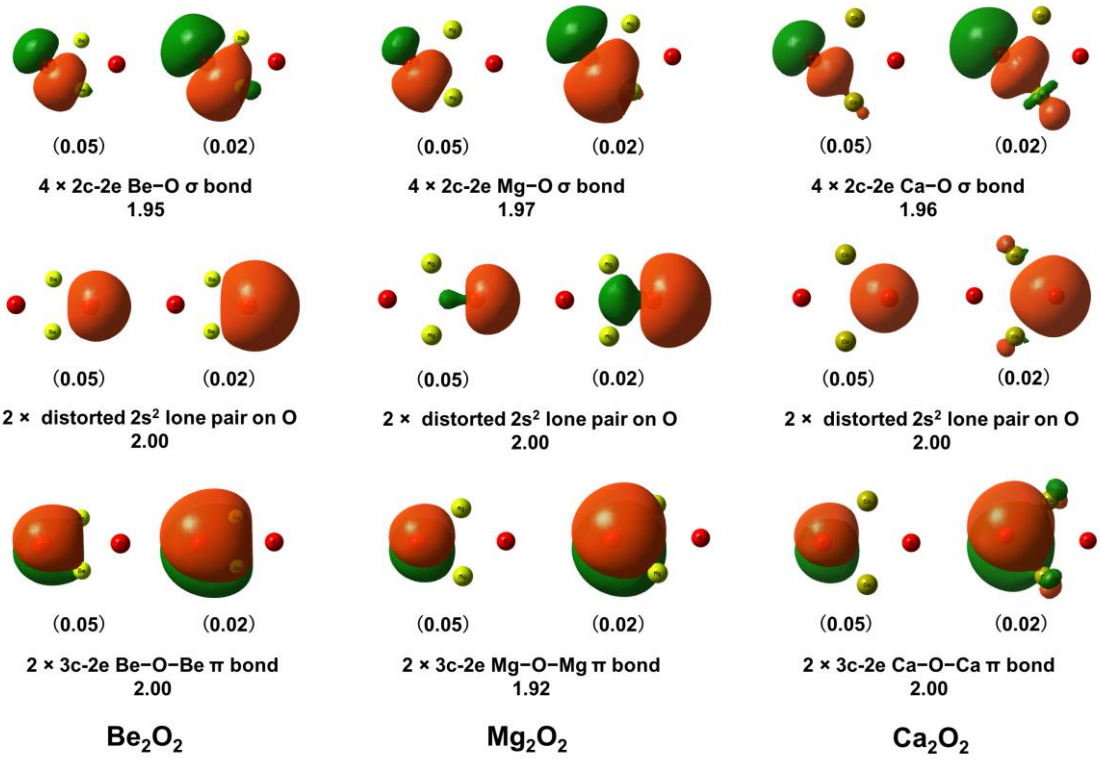
(0.05) (0.02)
4 × 2c-2e Be−O σ bond
1.95
(0.05) (0.02)
4 × 2c-2e Mg−O σ bond
1.97
(0.05) (0.02)
4 × 2c-2e Ca−O σ bond
1.96
(0.05) (0.02)
2 × distorted 2s² lone pair on O
2.00
(0.05) (0.02)
2 × distorted 2s² lone pair on O
2.00
(0.05) (0.02)
2 × distorted 2s² lone pair on O
2.00
(0.05) (0.02)
2 × 3c-2e Be−O−Be π bond
2.00
(0.05) (0.02)
2 × 3c-2e Mg−O−Mg π bond
1.92
(0.05) (0.02)
2 × 3c-2e Ca−O−Ca π bond
2.00
Be2O2
Mg2O2
Ca2O2

Figure 6

Table 1. Standard values for E-E (E = Be, Mg, Ca) single, double and triple bonds lengths [Å] according to ref. 1-3.

	Be-Be	Mg-Mg	Ca-Ca
Single	2.04	2.78	3.42
Double	1.80	2.64	2.94
Triple	1.70	2.54	2.66

Table 2. Bond dissociation energies D_e (kcal/mol) for the reaction $M_2O_2 \rightarrow 2$ MO and NBO atomic partial charges q and Wiberg bond orders P at the CCSD(T)/cc-pVQZ level.

	D_e	q(M)	q(O)	P(M-M)	P(M-O)
BeO	-	1.31	-1.31	-	1.16
Be_2O_2	162.7	1.37	-1.37	0.06	0.56
MgO	-	1.29	-1.29	-	1.05
Mg_2O_2	130.2	1.65	-1.65	0.03	0.32
CaO	-	1.52	-1.52	-	0.89
Ca_2O_2	121.5	1.61	-1.61	0.04	0.37

Table 3. EDA-NOCV results of E_2O_2 using the singlet (S) fragments EO (E = Be, Mg, Ca) at the BP86(D3)/TZ2P+ level of theory using the CCSD(T)/cc-pVTZ optimized geometries. . Energy values are given in kcal/mol.

Fragments	BeO (S) + BeO (S)	MgO (S) + MgO (S)	CaO (S) + CaO (S)
ΔE_{int}	-172.0	-132.5	-134.0
ΔE_{Pauli}	306.9	206.1	180.7
ΔE_{elstat}[a]	-269.7 (56.3%)	-218.6 (64.6%)	-195.5 (62.1 %)
ΔE_{orb}[a]	-208.0 (43.4%)	-118.1 (34.9%)	-117.3 (37.3 %)
ΔE_{disp}[a]	-1.2 (0.3%)	-1.9 (0.5%)	-1.9 (0.6 %)
$\Delta E_{orb(1)}$[b] (σ)	-93.4 (44.9%)	-43.6 (36.9%)	-34.2 (29.2 %)
$\Delta E_{orb(2)}$[b] (σ)	-45.6 (21.9%)	-42.0 (35.6%)	-27.0 (23.0 %)
$\Delta E_{orb(3)}$[b] (π)	-35.8 (17.2%)	-13.7 (11.6%)	-13.2 (11.3 %)
$\Delta E_{orb(4)}$[b] (σ)	-15.8 (7.6%)	-6.1 (5.2%)	-16.8 (14.3 %)
$\Delta E_{orb(5)}$[b] (π)	-7.9 (3.8%)	-4.7 (4.0%)	-11.4 (9.7 %)
$\Delta E_{orb(6)}$[b] (σ)	-5.4 (2.6%)	-5.7 (4.8%)	-11.1 (9.5 %)
$\Delta E_{orb(rest)}$	-4.1 (2.0%)	-2.3 (1.9%)	-3.6 (3.0 %)
ΔE_{prep}	15.5	5.0	25.9
ΔE^c (= $-D_e$)	-156.5	-127.5	-108.1

[a]The values in parentheses give the percentage contribution to the total attractive interactions $\Delta E_{elstat} + \Delta E_{orb} + \Delta E_{disp}$.

[b]The values in parentheses give the percentage contribution to the total orbital interactions ΔE_{orb}

[c]$\Delta E = \Delta E_{int} - \Delta E_{prep}$

TOC Graphic